Combined EZH2 Inhibition and IKAROS Degradation Leads to Enhanced Antitumor Activity in Diffuse Large B-cell Lymphoma

Kit I. Tong[1], Sharon Yoon[1,2], Keren Isaev[1], Mehran Bakhtiari[1], Tracy Lackraj[1], Michael Y. He[1], Jesse Joynt[1,2], Anjali Silva[1,3], Maria C. Xu[4], Gilbert G. Privé[1,5], Housheng Hansen He[1,5], Rodger E. Tiedemann[1,5], Elizabeth A. Chavez[6], Lauren C. Chong[6], Merrill Boyle[6], David W. Scott[6], Christian Steidl[6], and Robert Kridel[1,2,5]

ABSTRACT

Purpose: The efficacy of EZH2 inhibition has been modest in the initial clinical exploration of diffuse large B-cell lymphoma (DLBCL), yet EZH2 inhibitors are well tolerated. Herein, we aimed to uncover genetic and pharmacologic opportunities to enhance the clinical efficacy of EZH2 inhibitors in DLBCL.

Experimental Design: We conducted a genome-wide sensitizing CRISPR/Cas9 screen with tazemetostat, a catalytic inhibitor of EZH2. The sensitizing effect of *IKZF1* loss of function was then validated and leveraged for combination treatment with lenalidomide. RNA sequencing (RNA-seq) and chromatin immunoprecipitation sequencing analyses were performed to elucidate transcriptomic and epigenetic changes underlying synergy.

Results: We identified *IKZF1* knockout as the top candidate for sensitizing DLBCL cells to tazemetostat. Treating cells with tazemetostat and lenalidomide, an immunomodulatory drug that selectively degrades IKAROS and AIOLOS, phenocopied the effects of the CRISPR/Cas9 screen. The combined drug treatment triggered either cell-cycle arrest or apoptosis in a broad range of DLBCL cell lines, regardless of *EZH2* mutational status. Cell-line–based xenografts also showed slower tumor growth and prolonged survival in the combination treatment group. RNA-seq analysis revealed strong upregulation of interferon signaling and antiviral immune response signatures. Gene expression of key immune response factors such as *IRF7* and *DDX58* were induced in cells treated with lenalidomide and tazemetostat, with a concomitant increase of H3K27 acetylation at their promoters. Furthermore, transcriptome analysis demonstrated derepression of endogenous retroviruses after combination treatment.

Conclusions: Our data underscore the synergistic interplay between IKAROS degradation and EZH2 inhibition on modulating epigenetic changes and ultimately enhancing antitumor effects in DLBCL.

Introduction

Diffuse large B-cell lymphoma (DLBCL) is the most common lymphoma subtype, with an incidence of 5.6/100,000 per year (1). Identifying novel treatment strategies for DLBCL is a critical, unmet medical need. Indeed, relapse occurs in 40% of all patients and is typically associated with resistance to chemotherapy (2). At least 80% of all patients with refractory DLBCL ultimately die from lymphoma, given that second-line treatment regimens, including high-dose chemotherapy and autologous stem cell transplantation, lead to cure in only a minority of patients (2). Even cutting-edge new treatment modalities such as chimeric antigen receptor (CAR) T-cell therapy offer durable benefit to only a fraction of patients (3). For all these reasons, patients with relapsed DLBCL urgently need more efficacious treatment options.

Over the last decade, advances in next-generation sequencing technology have led to granular cataloguing of genetic alterations that are recurrent in B-cell lymphomas. A major theme is the common disruption of genes encoding histone modifiers. In 2010, *EZH2* was reported for the first time to be frequently mutated in both DLBCL and follicular lymphoma (4). EZH2 functions as a histone methyltransferase and is a component of the polycomb repressive complex 2 (PRC2), mediating repression of gene expression by promoting methylation of histone H3 on lysine 27 residues (5–7). Mutations in *EZH2* are predominantly gain-of-function hotspot mutations (8), with most mutations causing nonsynonymous amino acid changes of Y646. In non-malignant germinal center B cells, EZH2 represses terminal differentiation through a blockade of checkpoint genes and this phenotype is reinforced in lymphoma cells that harbor mutant *EZH2* (9). Because *EZH2* mutations were reported, several selective small-molecule inhibitors have been developed that compete with the substrate (S-adenosyl methionine) of the catalytic SET domain of EZH2 and, hence, inhibit its methyltransferase activity (10–13). The clinical efficacy of one of these compounds, tazemetostat, has been explored in a phase II trial (NCT01897571), with overall response rates of 69% reported in *EZH2*-mutated and 35% in wildtype follicular lymphoma, as well as 29% and 15% in *EZH2*-mutated and wildtype DLBCL, respectively (14, 15). Subsequently, based on the findings of this multicenter study, an accelerated approval for the use of tazemetostat for the treatment of adults with relapsed or refractory follicular lymphoma in conjunction with a companion diagnostic *EZH2* mutation test has been expedited (16).

[1]Princess Margaret Cancer Centre, University Health Network, Toronto, Ontario, Canada. [2]Institute of Medical Science, University of Toronto, Ontario, Canada. [3]Vector Institute, Toronto, Ontario, Canada. [4]University of Toronto Schools, Ontario, Canada. [5]Department of Medical Biophysics, University of Toronto, Ontario, Canada. [6]Centre for Lymphoid Cancer, BC Cancer, Vancouver, British Columbia, Canada.

Note: Supplementary data for this article are available at Clinical Cancer Research Online (http://clincancerres.aacrjournals.org/).

K.I. Tong, S. Yoon, and K. Isaev contributed equally to this article.

Corresponding Author: Robert Kridel, Medical Oncology and Hematology, Princess Margaret Cancer Centre, 101 College Street, Toronto, ON M5G 1L7, Canada. Phone: 416-946-2243; E-mail: robert.kridel@uhn.ca

Clin Cancer Res 2021;27:5401–14

doi: 10.1158/1078-0432.CCR-20-4027

Translational Relevance

Single-agent targeted therapies have suboptimal response rates in aggressive lymphoma, yet the design of rational combination strategies is hampered by the sheer number of possible combinations. Herein, through genome-scale CRISPR/Cas9 screening, we identified an epigenetic cross-talk between EZH2 inhibition and IKAROS degradation that can be leveraged to enhance antitumor effects. Our finding has translational relevance as EZH2 inhibitors have activity in a subset of germinal center-derived B-cell lymphomas and are well tolerated, hence ideally suited for exploring combination therapy strategies in the clinical setting. Moreover, our observation that combined targeting of EZH2 and IKAROS leads to an interferon response and transcriptional derepression of endogenous retroviruses provides additional preclinical support to ongoing studies exploring epigenetic sensitization to enhance the effects of immune therapies.

These observations document the potential for high efficacy in a subset of patients, partially identified by lymphoma subtype and *EZH2* mutational status. Nonetheless, it is unclear why not all patients with *EZH2*-mutated DLBCL or follicular lymphoma respond. In addition, given that tazemetostat is well tolerated, treatment efficacy can potentially be enhanced by combination therapy. The focus on inhibition of EZH2 is further justified by recent insight that the molecularly defined EZB subtype of DLBCL, characterized by frequent mutations of *EZH2* and translocations of *BCL2*, has poor outcome when compared to other germinal center B cell–like (GCB)-DLBCL cases (17, 18). To elucidate whether knockout of individual genes might confer sensitivity to tazemetostat (synthetic lethality), we performed a genome-wide knockout screen in SU-DHL-4 cells that are relatively resistant to EZH2 inhibition, despite harboring an *EZH2* mutation (10, 11, 19). We identified an interaction between EZH2 inhibition and IKAROS degradation that can be exploited for combinatorial therapeutic targeting in *EZH2*-mutated and wildtype models, and describe the transcriptomic and epigenetic underpinnings underlying synergy between tazemetostat and lenalidomide.

Materials and Methods

Cell lines

GCB-DLBCL cell lines used in this study with *EZH2* gain-of-function mutation were: SU-DHL-4 (RRID:CVCL_0539), SU-DHL-6 (RRID:CVCL_2206), RL (RRID:CVCL_1660), WSU-DLCL-2 (RRID:CVCL_1902), Karpas-422 (RRID:CVCL_1325), and OCI-Ly1 (RRID:CVCL_1879). Cell lines with *EZH2* wildtype status were: DOHH2 (RRID:CVCL_1179), SU-DHL-5 (RRID:CVCL_1735), and HT (RRID:CVCL_1290). SU-DHL-4, SU-DHL-6, RL, WSU-DLCL-2, Karpas-422, DOHH2, and OCI-Ly1 harbor a t(14;18) translocation, whereas SU-DHL-5 and HT do not. The cell lines SU-DHL-4, SU-DHL-6, WSU-DLCL-2, DOHH2, RL, HT, and OCI-Ly1 are derived from male patients, and SU-DHL-5 and Karpas-422 from female patients. Genetically modified SU-DHL-4-Cas9, SU-DHL-4-Cas9 deficient in IKAROS or AIOLOS, and SU-DHL-4-Cas9 LacZ gRNA control cell lines were generated as described in the Supplementary Materials and Methods. All cell lines (parental and engineered) were authenticated using short tandem repeat analysis and were routinely confirmed free of *Mycoplasma* contamination using the e-Myco VAliD mycoplasma PCR detection kit (FroggaBio).

Genome-scale CRISPR/Cas9 screen

A synthetic lethal CRISPR/Cas9 screen was performed using SU-DHL-4-Cas9 cells and Toronto KnockOut Library v1 (TKOv1; ref. 20) in the presence of 1 or 5 μmol/L tazemetostat (Selleckchem, catalog no. S7128) as the treatment arms and DMSO as the vehicle control arm over 14 days of cell propagation. After next-generation sequencing of the gRNA library, the differentially represented gRNAs (tazemetostat vs. DMSO) were identified using Model-based Analysis of Genome-wide CRISPR/Cas9 Knockout (MAGeCK; v0.5.7) and the candidate genes were determined on the basis of the modified robust rank aggregation (RRA) scores generated from the gRNA analysis (21).

Drug-treatment matrices and determination of synergy

The cell lines were treated with eight doses per drug or DMSO for 6 days. Cell viability was assessed by CellTiter-Glo luminescent cell viability assay (Promega, catalog no. G7572). Percent viability was determined by normalizing luminescent readouts to vehicle controls. Synergy scores were determined using the SynergyFinder R package (22).

In vivo experiments

SCID mice were subcutaneously injected with RL cells into the right flank. Once tumors were established, mice were randomly assigned to oral gavage with vehicle, lenalidomide (50 mg/kg twice daily, Sigma, catalog no. 901558), tazemetostat (EPZ-6438, 250 mg/kg twice daily) or their combination. EPZ-6438 was provided by Epizyme, Inc. Tumor volumes were measured daily throughout the experiment. This animal study was approved by the University Health Network Animal Care Committee.

RNA sequencing and data analysis

Drug- or DMSO-treated SU-DHL-4, RL, and SU-DHL-4-Cas9 deficient in IKAROS or LacZ gRNA control cell lines, were subjected to RNA sequencing (RNA-seq), as described in the Supplementary Materials and Methods. Differential gene expression analysis was performed in edgeR, with absolute log fold change (FC) > 2 and $P_{adjusted} < 0.05$ as cutoffs (23, 24). Pathway analysis was performed using g:Profiler (25, 26).

Chromatin immunoprecipitation sequencing and data analysis

The chromatin immunoprecipitation sequencing (ChIP-seq) samples were prepared from the drug- or DMSO-treated RL cells using the SimpleChIP Enzymatic Chromatin IP Kit (Cell Signaling Technology, catalog no. 9003). The next-generation sequencing reads were mapped to the hg19 reference genome using Burrows-Wheeler aligner v0.7.15 (27), filtered and QC checked by standard procedures. Peak calling was performed by MACS2 v2.1.0 (28). Differentially H3K27ac enriched peaks between treatment samples were identified by DiffBind (29). Promoters and putative enhancer regions were then annotated using ChIPseeker (30) with significant H3K27ac enrichment defined by absolute FC > 1 and FDR < 0.05, and comparison was made across samples. Significantly H3K27ac-enriched regions were further analyzed with the differential gene expression data from RNA-seq of the same RL cell line. Pathways associated with concomitant differentially upregulated genes and significant H3K27ac-enriched regions were identified using g:Profiler (25, 26).

Statistical analysis

All data points were represented as mean ± SD, with exception of the animal study in which tumor volumes were represented as mean ± SEM. Two-tailed unpaired Student *t* test was used to compare means

between two groups, as indicated in the figure legends and in figures. One-tailed Welch *t* test was used to compare response ratios to tazemetostat (in **Fig. 1E**). $P < 0.05$ was considered statistically significant. For transcriptome and epigenomic profiling analyses, genes and regions with FDR values < 0.05 were considered statistically significant.

Data availability

RNA-seq and ChIP-seq data have been deposited in the Gene Expression Omnibus under accession number GSE152069.

Additional methods

Detailed methods for CRISPR/Cas9 screen and analysis, cell culture, generation of *IKZF1* and *IKZF3* knockout cell lines, Western blot analysis, cell counting, drug-treatment synergy matrices assay, *in vivo* experiment, BrdU proliferation assay, apoptosis assay, quantitative real-time polymerase chain reaction (qRT-PCR), RNA-seq, co-immunoprecipitation, ChIP-seq, ChIP quantitative PCR (ChIP-qPCR), immunostaining and microscopy, and transcriptomic and epigenomic data analyses are described in the Supplementary Materials and Methods.

Results

IKZF1 knockout sensitizes SU-DHL-4 cells to tazemetostat

To address whether knockout of individual genes might confer sensitivity to tazemetostat in relatively resistant, but *EZH2*-mutated DLBCL cell lines (synthetic lethality), we performed a genome-scale CRISPR/Cas9 knockout screen in SU-DHL-4 cells. These cells were transduced with the Toronto KnockOut v1 library (20) and exposed to either tazemetostat (1 and 5 μmol/L) or vehicle (DMSO) for 14 days in triplicate (**Fig. 1A**). The quality of the screen was well suited for downstream analysis, with a mean number of mapped reads of 16.3M per sample and a low mean Gini index of 0.096, suggesting even distribution of read counts (Supplementary Fig. S1A and S1B). Unsupervised clustering showed grouping of samples by treatment condition, as expected (Supplementary Fig. S1C). Comparing DMSO-treated cells with cells from day 0 (essentiality screen), we identified 3,432 essential genes (FDR < 0.05), with *BCL2* being the top candidate (FDR = 1.8×10^{-5}; Supplementary Fig. S2A). This set of essential genes significantly overlapped with results from a similar screen performed in SU-DHL-4 cells by Reddy and colleagues (ref. 31; hypergeometric $P = 2.01 \times 10^{-316}$; Supplementary Fig. S2B), underlining the robustness of our experimental approach to identify gene dropout. Next, to identify synthetic lethality, we compared tazemetostat-treated cells (5 μmol/L) with cells treated with DMSO (synthetic lethality screen). Five candidate genes were identified as being negatively selected (FDR < 0.05), with the top one being *IKZF1* (RRA score = 2.04×10^{-9}, $P = 2.87 \times 10^{-7}$, FDR = 0.005), encoding the Ikaros family zinc finger 1 (IKAROS), followed by *EGLN1, C18orf8, DOT1L*, and *EFNB2* (**Fig. 1B** and **C**; Supplementary Table S1). The gRNAs targeting another Ikaros family zinc finger members, *IKZF3*, encoding the AIOLOS transcription factor, had a trend toward depletion (RRA score = 0.003, $P = 0.005$, FDR = 0.349). Findings were similar when comparing cells treated with 1 μmol/L tazemetostat to DMSO-treated cells, with two genes identified (FDR < 0.05), including *IKZF1* (RRA = 1.09×10^{-6}, $P = 4.88 \times 10^{-6}$, FDR = 0.042). Neither *IKZF1* nor *IKZF3* were among the top essential genes (ranks 2,346 and 6,844, respectively), suggesting that the negative selective pressure conferred by their knockout was observed predominantly when EZH2 was inhibited. Individual CRISPR/Cas9-mediated knockout of *IKZF1* and *IKZF3* recapitulated decreased fitness when SU-DHL-4 cells were exposed to tazemetostat, with a response ratio below 1, in keeping with sensitization (**Fig. 1D** and **E**), thus validating the findings from the genome-scale library screen.

Lenalidomide and tazemetostat synergize to reduce cellular proliferation in DLBCL cell lines

As IKAROS and AIOLOS are selectively degraded by lenalidomide through a cereblon-dependent mechanism (32, 33), we explored whether the effect of tazemetostat on cell survival and/or proliferation could be enhanced by combination with lenalidomide. Combined drug treatment sensitized SU-DHL-4 cells to the effect of tazemetostat, which was most pronounced after 10–14 days (**Fig. 1E**). Using dose–response drug matrices incubated over 6 days, we observed synergy that was most pronounced in RL cells (mean Bliss score 30.5), SU-DHL-5 (16.2), SU-DHL-4 (15.0), and HT (8.1; **Fig. 2A** and **B**). High synergy scores were observed in both *EZH2*-mutant (RL, SU-DHL-4) and *EZH2*-wildtype cell lines (HT, SU-DHL-5). As expected, we confirmed decreased expression of IKAROS protein after treatment with lenalidomide, and decreased H3K27me3 levels with tazemetostat (Supplementary Fig. S3A–S3C). These effects were also observed with combination treatment. As an orthogonal readout of cell growth, we performed proliferation assays and found that the addition of lenalidomide to tazemetostat significantly reduced cell proliferation in RL, WSU-DLCL-2, SU-DHL-5, and HT (**Fig. 2C**; Supplementary Fig. S4). Moreover, the frequency of apoptosis and/or necrosis was significantly increased in two of these four cell lines (WSU-DLCL-2 and HT; Supplementary Fig. S5). Furthermore, to test whether combination treatment has *in vivo* efficacy, we xenografted RL cells in the right flank of 40 SCID mice (2.5 million RL cells per mouse) that were then randomized to DMSO control treatment, single-agent tazemetostat (250 mg/kg orally twice daily), single-agent lenalidomide (50 mg/kg orally twice daily), or combination treatment. Mice in the combination treatment group experienced slower tumor growth ($P < 0.001$; **Fig. 2D**) and had prolonged survival ($P = 0.021$; **Fig. 2E**). These observations confirm that combination treatment with tazemetostat and lenalidomide has enhanced *in vitro* and *in vivo* antitumor activity, compared with either single agent alone. This finding was unexpected, given that *EZH2* gain-of-function alterations are predominantly seen in GCB-DLBCL, whereas lenalidomide is considered to have most pronounced activity in activated B-cell–like (ABC)-DLBCL (34).

Gene expression changes associated with combination treatment

We presumed that the phenotypic effects observed with combination treatment resulted primarily from the removal of a differentiation blockade imposed by EZH2 and IKAROS. To examine this hypothesis, we applied a NanoString assay that provides digital gene expression counts of ABC and GCB-DLBCL genes to four cell-line models: SU-DHL-4, RL, and HT cells treated alone, with tazemetostat, with lenalidomide, or with combination, and SU-DHL-4 cells, with and without isogenic *IKZF1* knockout, treated with tazemetostat. Out of the eight ABC genes that are part of the Lymph2Cx cell of origin classifier, two genes (*TNFRSF13B* and *CREB3L2*) were upregulated with combination treatment ($P_{adjusted} < 0.001$ and 0.013, respectively). On the other hand, *IRF4*, encoding a master transcription factor that establishes plasma cell identity, was not differentially expressed, and one of the seven GCB genes from the Lymph2Cx assay (*MAML3*) was significantly upregulated with combination treatment. Taken together, these results did not definitively support differentiation toward an ABC phenotype as underlying the phenotypic effects observed with combination treatment.

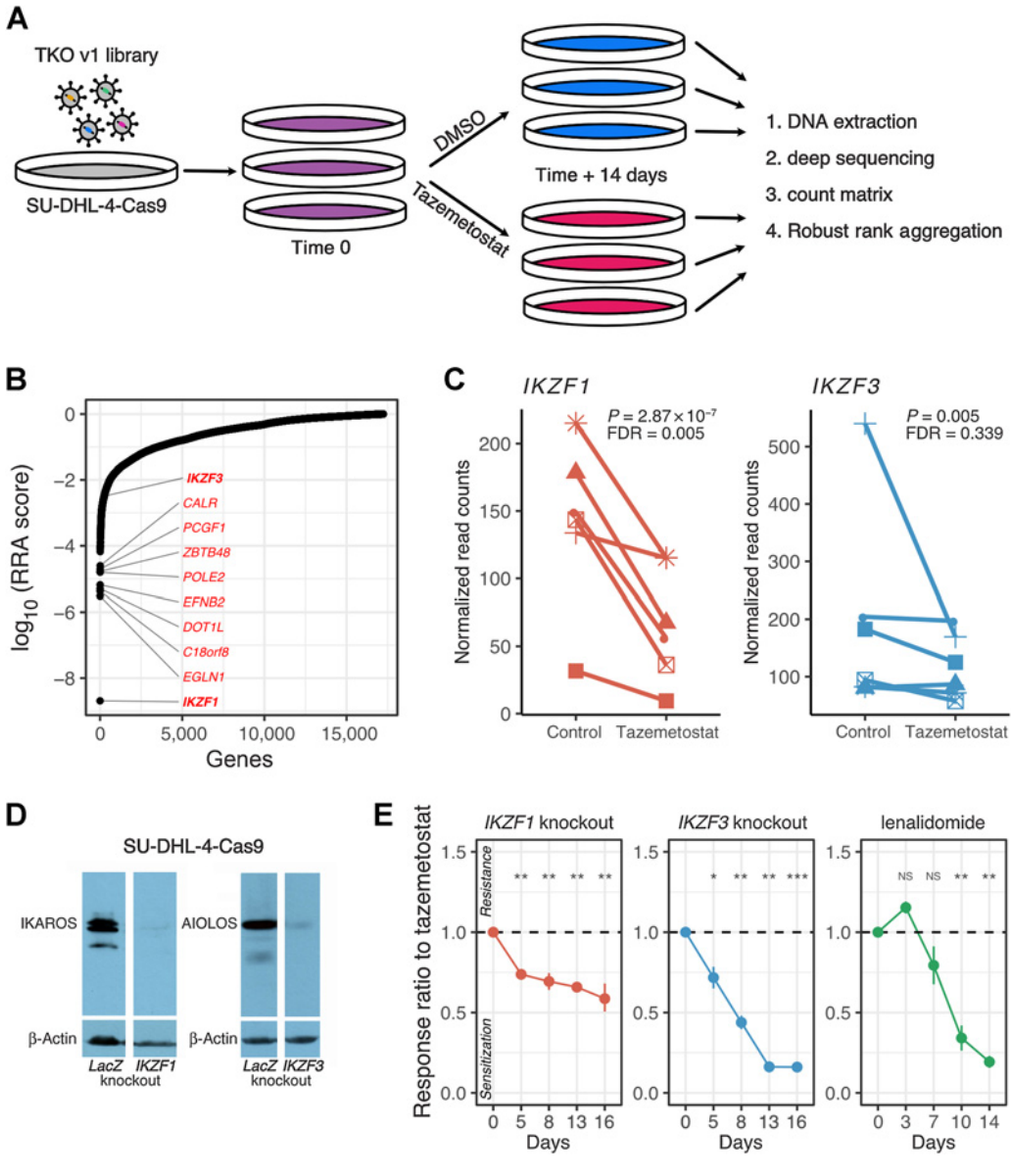

Figure 1.

CRISPR screen identifies that the loss of *IKZF1* or *IKZF3* sensitizes DLBCL cells to tazemetostat. **A,** Schematic diagram depicting the workflow of the genome-wide TKOv1 gRNA library CRISPR/Cas9 screen in the SU-DHL-4 DLBCL cell line stably expressing the SpCas9 nuclease. **B,** MAGeCK's RRA score graph showing the negatively selected candidates, at the gene level. **C,** Normalized number of sequencing read counts of each gRNA targeting the indicated gene in cells cultured in the presence of DMSO (control) or 5 μmol/L tazemetostat over 14 days. **D,** Western blot analysis showing depletion of either IKAROS or AIOLOS protein in the respective SU-DHL-4-Cas9 knockout cell lines. SU-DHL-4-Cas9 cells transduced with gRNA against the *LacZ* gene served as control. **E,** *IKZF1* or *IKZF3* gene knockout SU-DHL-4-Cas9 cells were cultured in the presence of DMSO or 5 μmol/L tazemetostat for 16 days. The rightmost panel shows results for SU-DHL-4 cells treated with tazemetostat and lenalidomide compared to single-agent drugs. A response ratio below 1 indicates sensitization (see Supplementary Materials and Methods). Data points show the mean response ratio and error bars show SD ($n = 3$ technical replicates). *P* values, one-tailed Welch *t* test on $\log_2$-transformed ratios (NS, not significant; *, $P < 0.05$; **, $P < 0.01$; ***, $P < 0.001$).

Thus, we performed RNA-seq to gain additional insight into transcriptional footprints underlying the various treatment conditions. Combination treatment resulted in the highest number of differentially expressed genes, compared with single-agent treatment (**Fig. 3A**). The various treatment conditions resulted in a higher number of upregulated versus downregulated genes, in keeping with derepression of gene expression. The number of differentially expressed genes was higher for the RL cell line, compared with SU-DHL-4, paralleling the higher degree of synergy in RL compared with SU-DHL-4. However, all pairwise overlaps of upregulated and downregulated genes were significant, suggesting consistent gene expression changes across cell lines (**Fig. 3B**; Supplementary Fig. S6). To characterize gene expression changes in light of lymphoid gene signatures, we performed functional enrichment analysis using a well-characterized database of gene sets encompassing B- and T-cell maturation (17). Among the top upregulated gene sets, the most

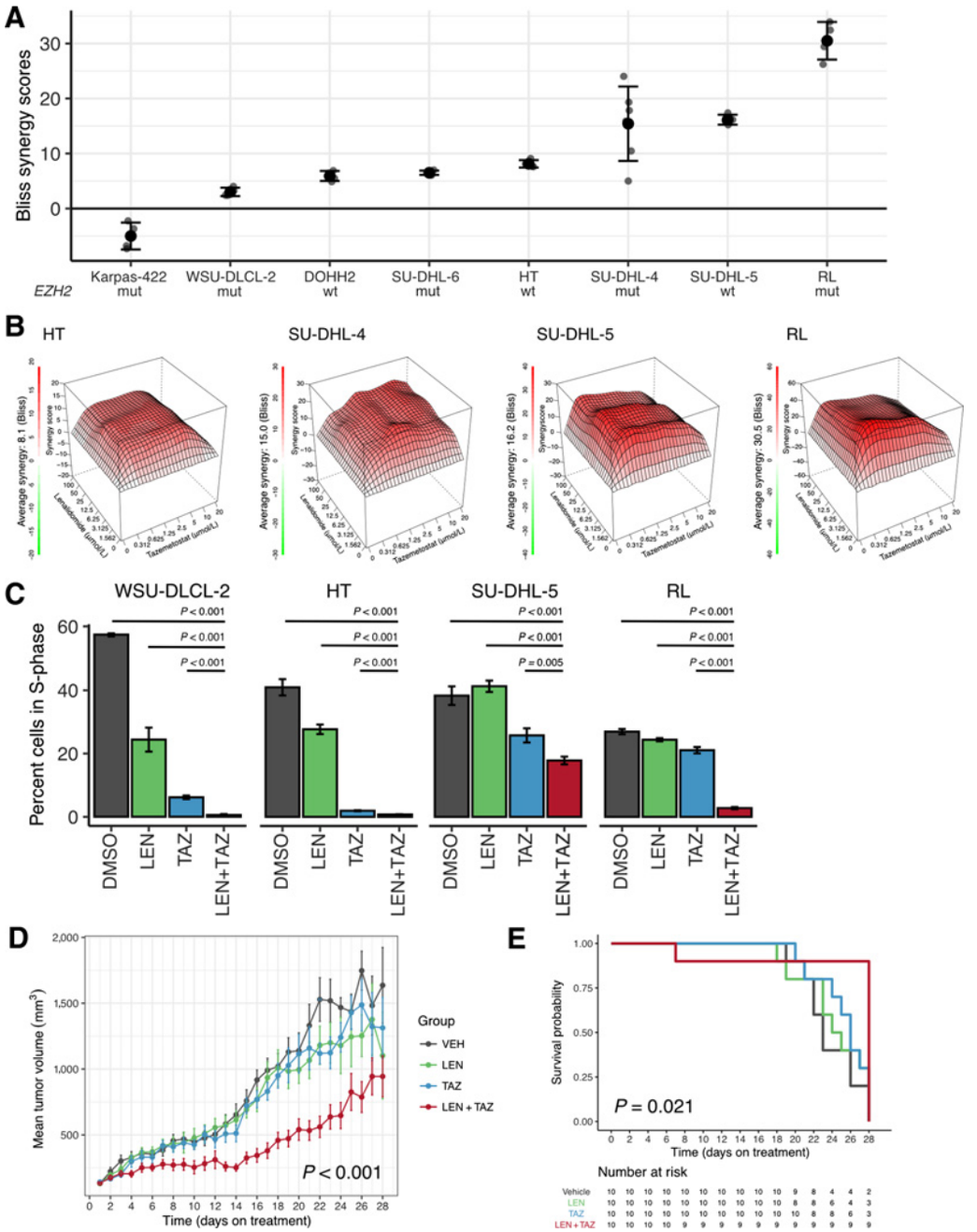

Figure 2.

Lenalidomide-induced degradation of IKAROS synergizes with the treatment of tazemetostat to reduce cell proliferation of DLBCL cell lines. **A,** GCB-DLBCL cell lines with or without *EZH2* gain-of-function mutation were cultured for 6 days in a dose–response matrix prepared with lenalidomide–tazemetostat drug pair to assess effects of the drug combination at increasing dose levels. Cellular ATP level or percent viability was assessed by CellTiterGlo and luminescent readout was normalized to DMSO vehicle control. Synergy score was obtained by implementing the SynergyFinder R package (v. 2.2.4) and applying the Bliss independence model. Data shown are mean ± SD of 2–3 independent experiments, each containing two technical replicates. All data points are depicted. **B,** Representative visualization of the synergy scores of four GCB-DLBCL cell lines with varying synergy scores. Drug concentration and synergy scores for each condition in the matrices were as shown. **C,** GCB-DLBCL cell lines were cultured with DMSO, 10 μmol/L lenalidomide (LEN), 5 μmol/L tazemetostat (TAZ), or 5 μmol/L tazemetostat + 10 μmol/L lenalidomide (LEN+TAZ) for 5 days. Percentage of S-phase (BrdU positive) population for each cell line and treatment condition was then analyzed by BrdU proliferation flow cytometry assay. Data shown are mean ± SD ($n = 3$ technical replicates). *P* values, two-tailed unpaired Student *t* test. **D,** Average tumor volumes for 40 SCID mice inoculated with RL cells in four treatment groups. Mice were treated by oral gavage with vehicle, lenalidomide (50 mg/kg twice daily), tazemetostat (250 mg/kg twice daily), or combination, and sacrificed when tumors reached a volume endpoint > 1,766 mm^3 or on day 28 (whichever occurred first). Data shown as mean values ± SEM, $n \leq 10$ per group. **E,** Overall survival of mice.

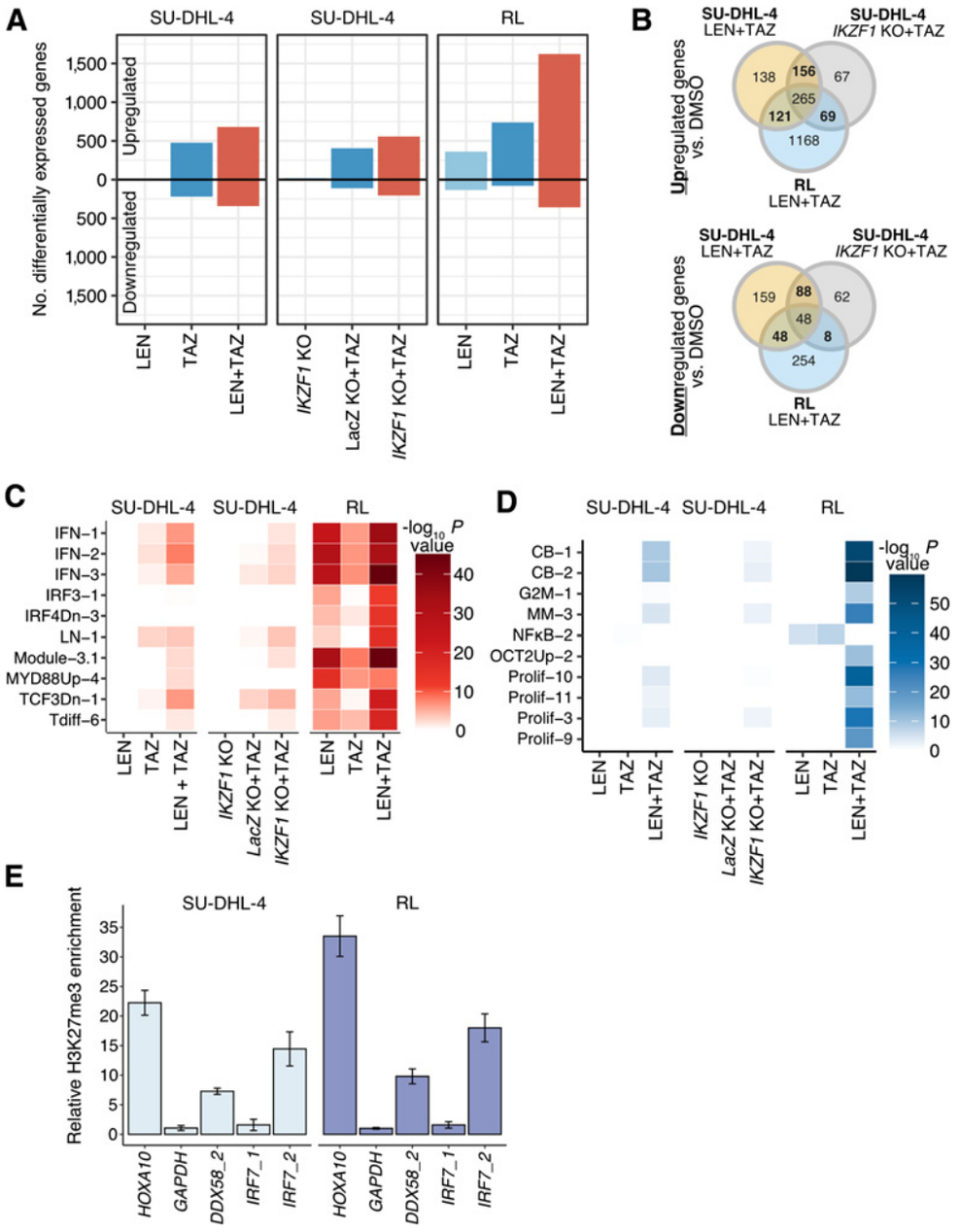

Figure 3.

Combination treatment perturbs gene expression and upregulates IFN signaling pathway. **A,** Three DLBCL model systems of SU-DHL-4 parental cells, SU-DHL-4-Cas9 *IKZF1* knockout cells or LacZ controls, and RL parental cells were treated with 5 μmol/L tazemetostat (TAZ), 10 μmol/L lenalidomide (LEN), or 5 μmol/L tazemetostat + 10 μmol/L lenalidomide (LEN+TAZ) for 6 days. Bar chart showing the number of differentially upregulated or downregulated genes in drug-treated cells relative to the gene expression in cells treated with DMSO or the LacZ controls. Data were generated from two technical replicates. **B,** Venn diagrams showing the number of differentially upregulated or downregulated genes, described as in **A**, overlapped or distinct among the three DLBCL model systems. **C,** Pathway analysis revealed lymphoid gene signatures with enrichment of IFN gene signature within the upregulated genes across the three model systems. **D,** Centroblastic and proliferation gene signatures were enriched within the downregulated genes. **E,** ChIP-qPCR assay showing enrichment of H3K27me3 within the promoters of *IRF7* and *DDX58*. Enrichment signal was normalized by input chromatin and expressed relative to a H3K27me3 negative region at the promoter of *GAPDH*. *HOXA10* is a H3K27me3 positive control region. Data shown are mean ± SD ($n = 3$ technical replicates).

consistent signal was observed for interferon (IFN) signatures, an effect that was mostly observed with combination treatment (**Fig. 3C**; Supplementary Table S2). Of interest, a signature of IFN genes that are repressed by IRF4 (IRF4Dn-3; ref. 34) was enriched in RL cells treated with lenalidomide, and even more so with combination treatment. We observed only modest enrichment of signatures reflective of NFκB signaling, further suggesting that terminal differentiation was not the main driver underlying the phenotypic effects seen with combination

treatment. On the other hand, centroblastic and proliferation signatures were significantly enriched within downregulated genes (**Fig. 3D**), mirroring findings from the proliferation experiments. Leveraging Gene Ontology, Reactome, and WikiPathways databases, we observed similar signals of IFN and cell adhesion pathways being enriched in upregulated genes, and cell-cycle transition and protein translation pathways being enriched in downregulated genes (Supplementary Fig. S7A and S7B; Supplementary Table S3). Using qRT-PCR, we observed robust upregulation of the interferon pathway members *IRF7* and *DDX58* with combination treatment, compared with either single-agent lenalidomide or tazemetostat, in five of seven cell lines tested (Supplementary Fig. S8A). While combination treatment did not lead to upregulation of *IRF7* and *DDX58* in the SU-DHL-4 cell line, several other inflammatory genes were upregulated in SU-DHL-4 based on RNA-seq (e.g., *IFI44, IFI6, IFIT1, IFIT3;* Supplementary Fig. S8B). In summary, our gene expression analysis provided support for upregulation of IFN signaling as a major transcriptional footprint underlying the synergistic activity of tazemetostat and lenalidomide.

Gene expression changes correlating with H3K27me3 regions and IKAROS binding sites

While we observed upregulation of IFN response pathways in combination treatment, the mRNA levels of IFNs (IFNα, IFNβ, and IFNγ) were not expressed above baseline in any of the treatment conditions across our three cell-line models. Thus, we predicted that upregulation of IFN-stimulated genes did not result from autocrine or paracrine secretion of cytokines but rather from epigenetic regulation. To answer this question, we overlaid the transcriptomic footprints that we had observed with publicly available ChIP-seq datasets, including H3K27me3 regions defined in *EZH2*-mutant DLBCL cell lines, and IKAROS binding sites in K562 and GM12878 cell lines (Supplementary Materials and Methods). We first evaluated whether there was a significant overlap between H3K27me3 and IKAROS binding. We annotated both peak sets and included only those annotated as promoters and within 2,000 bp of transcription start sites. Significant overlap was observed where 63% of H3K27me3 and 33% of IKAROS peaks overlapped ($P = 0.001$; Supplementary Fig. S9A). Significant overlap had also been previously observed in B-cell acute lymphoblastic leukemia (35). We next evaluated how genes annotated to these peaks related to the differential expression program we observed following tazemetostat and lenalidomide treatment (Supplementary Fig. S9B). We saw that significantly upregulated genes were strongly associated with H3K27me3. In the RL cell line, significantly upregulated genes were also associated with IKAROS binding sites.

As IKAROS and H3K27me3 are partially associated, we further annotated differentially expressed genes as overlapping both IKAROS and H3K27me3, IKAROS alone, H3K27me3 alone, or neither. We observed that the relative overlap of gene promoters with H3K27me3 or H3K27me3/IKAROS was greater for upregulated than for downregulated genes (60% vs. 38%, χ^2 $P < 0.001$), for both the RL and SU-DHL-4 cell lines. Furthermore, the number of upregulated genes overlapping H3K27me3 was higher in tazemetostat-treated cells compared with lenalidomide, as expected (Supplementary Fig. S9C). Meanwhile, downregulated genes were enriched in regions marked by IKAROS alone or by neither mark, when compared with upregulated genes. We then explored the association between H3K27me3 regions/IKAROS binding sites and pathway enrichment analysis. The highest number of pathways was identified as being enriched within upregulated genes overlapping both H3K27me3 and IKAROS marks (Supplementary Fig. S9D). IFN-related pathways were most significantly upregulated within genes overlapping both H3K27me3 and IKAROS, as well as within genes overlapping IKAROS alone (Supplementary Fig. S9E). We validated enrichment of H3K27me3 in the promoter regions of *IRF7* and *DDX58* using ChIP-qPCR (**Fig. 3E**). Meanwhile, proliferation signatures were found to be downregulated within genes across all H3K27me3/IKAROS combinations, except for those genes marked by H3K27me3 alone (i.e., without evidence of IKAROS binding; Supplementary Fig. S9E). Taken together, our findings illustrate that pathways underlying synergy are intimately associated with direct epigenetic changes mediated by EZH2 inhibition and IKAROS degradation.

IKAROS and histone deacetylation

As IKAROS is not known to directly modify histones, we sought to explore its interactions with protein partners that remodel chromatin. Physical interactions between IKAROS and the nucleosome remodeling deacetylase (NuRD) complex, underlying histone deacetylation via histone deacetylases 1 and 2 (HDAC1 and HDAC2), have been well characterized, especially in the context of normal T-cell development and acute lymphoblastic leukemia (35, 36). Overall, such interactions are less established in the mature B-cell context, although one study has found evidence of an interaction between AIOLOS/IKAROS and HDAC1 and HDAC2 using protein ligation studies (37). In keeping with a potential role for the NuRD complex in the synergistic effects we observed, we found that two members of this complex had signal toward depletion from tazemetostat-treated SU-DHL-4 cells in our CRISPR-Cas9 knockout screen: *MBD2* (encoding methyl-CpG binding domain protein 2; $P = 5.90 \times 10^{-4}$, FDR = 0.186) and *HDAC1* ($P = 1.13 \times 10^{-3}$, FDR = 0.202). Interestingly, gRNAs against *HDAC3* (encoding HDAC3 that associates with the SMRT/NCOR complex) were not depleted in the library screen, and were significantly enriched ($P = 3.49 \times 10^{-10}$, FDR $= 2.87 \times 10^{-7}$), similarly to *NCOR1* ($P = 2.82 \times 10^{-10}$, FDR $= 2.87 \times 10^{-7}$; **Fig. 4A**). We could confirm an antagonistic effect between EZH2 and HDAC3 inhibition in SU-DHL-4 cells using small molecule inhibitors of EZH2 (5 μmol/L tazemetostat) and HDAC3 (1 μmol/L RGFP966; **Fig. 4B**). However, this effect was exclusively observed in SU-DHL-4 cells, when compared with three other cell lines (RL, OCI-Ly1, and DOHH2). Moreover, annotating H3K27me3 peaks with an exhaustive dataset of transcriptional regulators (ReMap 2020), we found evidence for enrichment of HDAC1, HDAC2, and IKAROS, in addition to EZH2 and BCL6 (positive controls), whereas HDAC3 was negatively associated with H3K27me3 (**Fig. 4C**). Co-immunoprecipitation confirmed a physical interaction between IKAROS and HDAC1 (**Fig. 4D**), as expected from the prior literature (38). Altogether, these observations suggest distinct interactions for various histone deacetylase enzymes and point toward a possible role of histone acetylation, mediated by decreased activity of the NuRD complex, underlying the gene expression changes observed with synergy.

Coordinated gene expression and chromatin acetylation changes underlying synergy

Thus, we sought to examine changes in H3K27 acetylation (H3K27ac), motivated also by the consideration that we observed a larger number of upregulated, compared with downregulated genes in combination treatment. Indeed, this mark has been associated with active enhancers in general (39), as well as with chromatin remodeling underlying IFN-induced expression of inflammatory genes specifically (40). We performed ChIP-seq for H3K27ac in the RL cell line and compared the distribution of significantly acetylated peaks between each treatment group and DMSO control (**Fig. 5A**; Supplementary

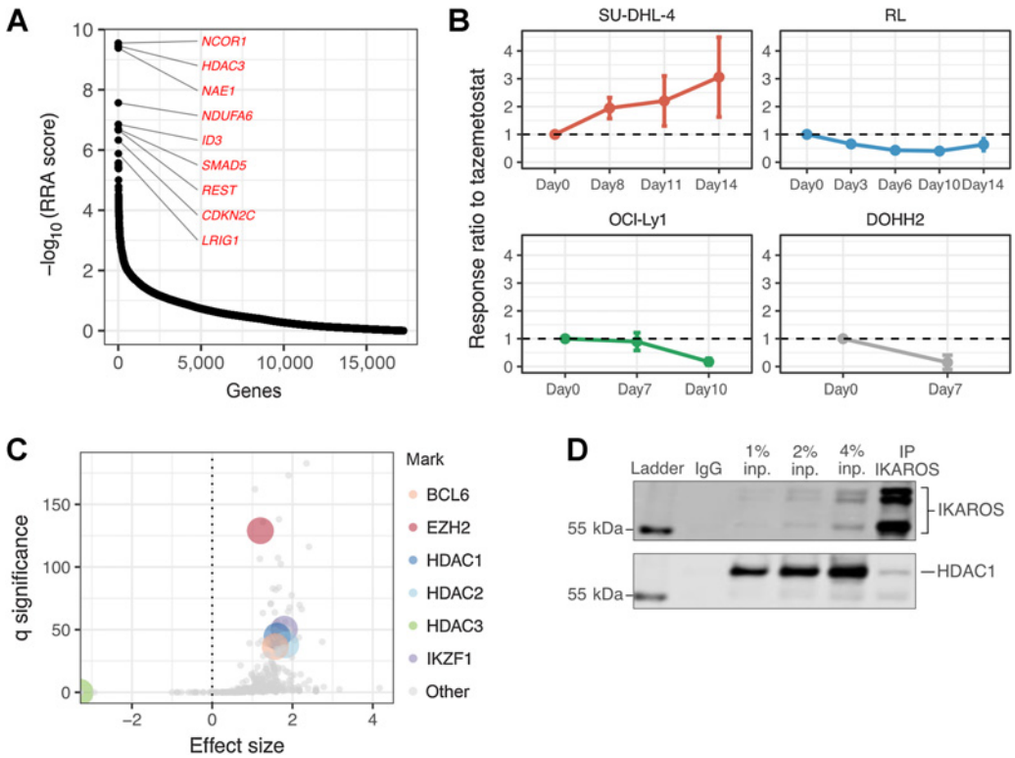

Figure 4.

Opposing effects of IKAROS and HDAC3 knockout/inhibition in response to EZH2 inhibition in the SU-DHL-4 cell line and association between H3K27me3 regions and HDAC1/2 deacetylases. **A,** MAGeCK's RRA score graph showing the positively selected candidates, at the gene level, from the genome-wide TKOv1 gRNA library CRISPR/Cas9 screen in the SU-DHL-4 DLBCL cell line treated with 5 μmol/L tazemetostat. **B,** Antagonistic effect between EZH2 and HDAC3 inhibition in SU-DHL-4 cell line, but not other DLBCL cell lines tested. Cells were incubated in the presence of DMSO, 5 μmol/L tazemetostat, 1 μmol/L RGFP966, or combination of both drugs. **C,** Enrichment of curated transcription factor peaks from ReMap 2020 within H3K27me3 regions defined in Donaldson-Collier and colleagues (61). Transcription factors of interest (HDAC1, HDAC2, HDAC3, IKZF1) and positive controls (EZH2, BCL6) are indicated in color. **D,** Co-immunoprecipitation (IP) of HDAC1 after IKAROS pull-down in RL cells. Immunoprecipitated complexes were resolved by SDS-PAGE followed by immunoblot analysis using specified antibodies. Isotype-matched IgG was used as a negative control for non-specific immunoprecipitation. Control input samples represent 1%, 2%, and 4% of total lysates prior to co-immunoprecipitation.

Fig. S10). The highest number of differentially acetylated peaks was found in combination treatment (13,463 increased and 10,276 decreased peaks). In the comparison of differential peaks between treatment groups, the largest overlap was observed between combination and tazemetostat treatment. Next, we assessed the strength of the acetylation signals by comparing FCs between treatment groups, and across both promoters and enhancers. We observed the highest median FCs in combination treatment, and this effect was most pronounced for enhancers (**Fig. 5B**). Importantly, FCs of upregulated peaks were significantly higher than those of deacetylated peaks (Wilcoxon test, $P < 0.05$), suggesting that acetylation signals were stronger than deacetylation signals.

The integration of acetylation with gene expression data revealed coordinated increases in H3K27ac and gene expression in all three treatment groups, when compared with DMSO, an effect that was most pronounced in combination treatment (**Fig. 5C** and **D**; Supplementary Fig. S11A). Increased acetylation at promoters accounted for 27%, 27%, and 29% of genes upregulated in lenalidomide-, tazemetostat-, and combination-treated cells, respectively. Genes involved in the upregulated pathways defined by both increased promoter H3K27 acetylation and gene expression included *NLRC5, IRF7, DDX58, IRF1*, and *STAT1*, which encode for effector proteins involved in antiviral immunity and cytokine response (Supplementary Fig. S11B). We further confirmed that the upregulated genes with increased acetylation were enriched in the pathways observed in **Fig. 3C**, including defense response to virus and IFN signaling (**Fig. 5E**; Supplementary Table S4). Conversely, the significantly downregulated genes in combination treatment with depleted H3K27ac peaks were enriched in the "sister chromatid segregation" and "mitotic spindle checkpoint" gene sets (**Fig. 5F**). This trend was not observed in lenalidomide or tazemetostat treatment alone, in keeping with a synergistic effect. The increase of H3K27ac deposition at the promoters of *IRF7, DDX58*, and *NLRC5* (**Fig. 5G**; Supplementary Fig. S12) was further validated by ChIP-qPCR assay (**Fig. 5H**). Thus, the differentially expressed genes observed in combination treatment are associated with complementary changes in H3K27ac.

ERV expression changes correlate with synergy and IFN response

Given that derepression of endogenous retroviruses (ERV) has previously been associated with viral response and interferon pathways in the context of epigenetic modulation (41–43), we investigated whether combination treatment influenced ERV expression in our RNA-seq dataset. We used Telescope (44) to annotate the expression

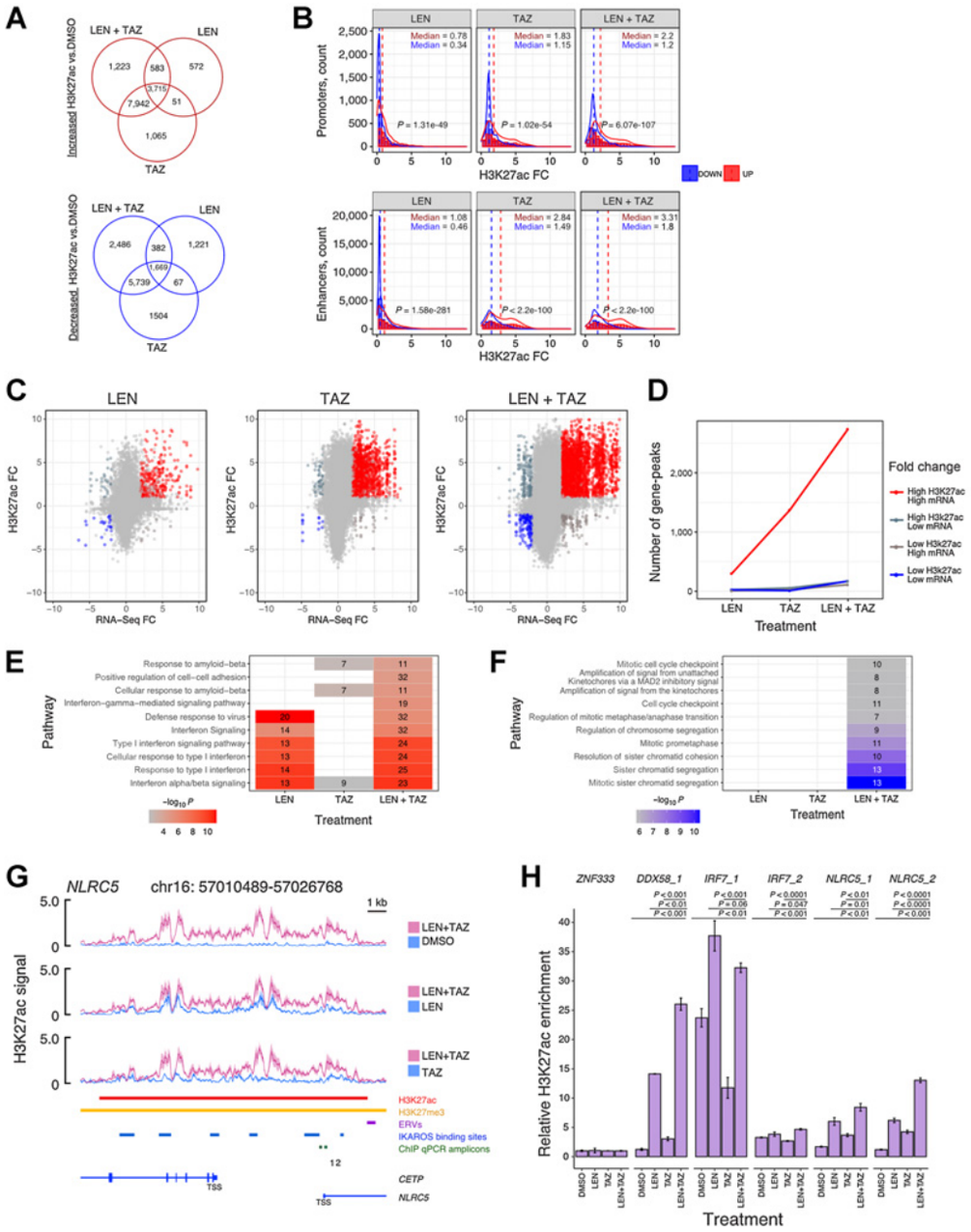

Figure 5.

Coordinated alteration in gene expression and chromatin acetylation underlies the synergy of drug combination. **A,** The overlap of H3K27ac peaks detected upon tazemetostat (TAZ), lenalidomide (LEN), or combination (LEN+TAZ) treatment for enriched and depleted regions. **B,** FCs summarized for H3K27ac peaks identified to be significant in at least one treatment. Median FC values are shown for enriched and depleted peaks across each treatment for peaks annotated as promoters (top) and enhancers (bottom). **C,** Summary of significant H3K27ac peaks across each treatment comparing the RNA-seq log FC for genes predicted to be associated with a given peak (*x*-axis) versus that peak's FC obtained from DiffBind (*y*-axis). **D,** Summary of the number of H3K27ac peak–gene pairs obtained in each of the four quadrants across the three treatments pertaining to **C**. **E,** Summary of the top pathways enriched by genes with significantly increased gene expression and increased levels of H3K27ac across each treatment. Numbers in tiles represent the number of genes found to be enriched in a given pathway. **F,** Summary of the top pathways enriched by genes with significantly decreased gene expression and reduced levels of H3K27ac across each treatment. **G,** Genomic view of a region spanning the *NLRC5* promoter region (hg19) on chromosome 16. H3K27ac signal represents MACS2 score obtained for each treatment along the MACS2 defined peaks. H3K27me3 represents publicly available peak data from *EZH2*-mutant DLBCL cell lines. ERVs represent ERV elements annotated by RepeatMasker. IKAROS binding sites are shown based on data from ENCODE. Regions amplified by ChIP quantitative PCR from *NLRC5* are as shown. **H,** ChIP quantitative PCR of H3K27 acetylation enrichment at promoter regions of *DDX58, IRF7*, and *NLRC5* genes in RL cells treated with DMSO, 5 μmol/L tazemetostat (TAZ), 10 μmol/L lenalidomide (LEN), or 5 μmol/L tazemetostat + 10 μmol/L lenalidomide (LEN+TAZ) for 3 days. H3K27 acetylation enrichment was expressed relative to a negative control region at the 3′ region of the *ZFN333* gene. Data shown are mean ± SD ($n = 3$ technical replicates). *P* values, two-tailed unpaired Student *t* test.

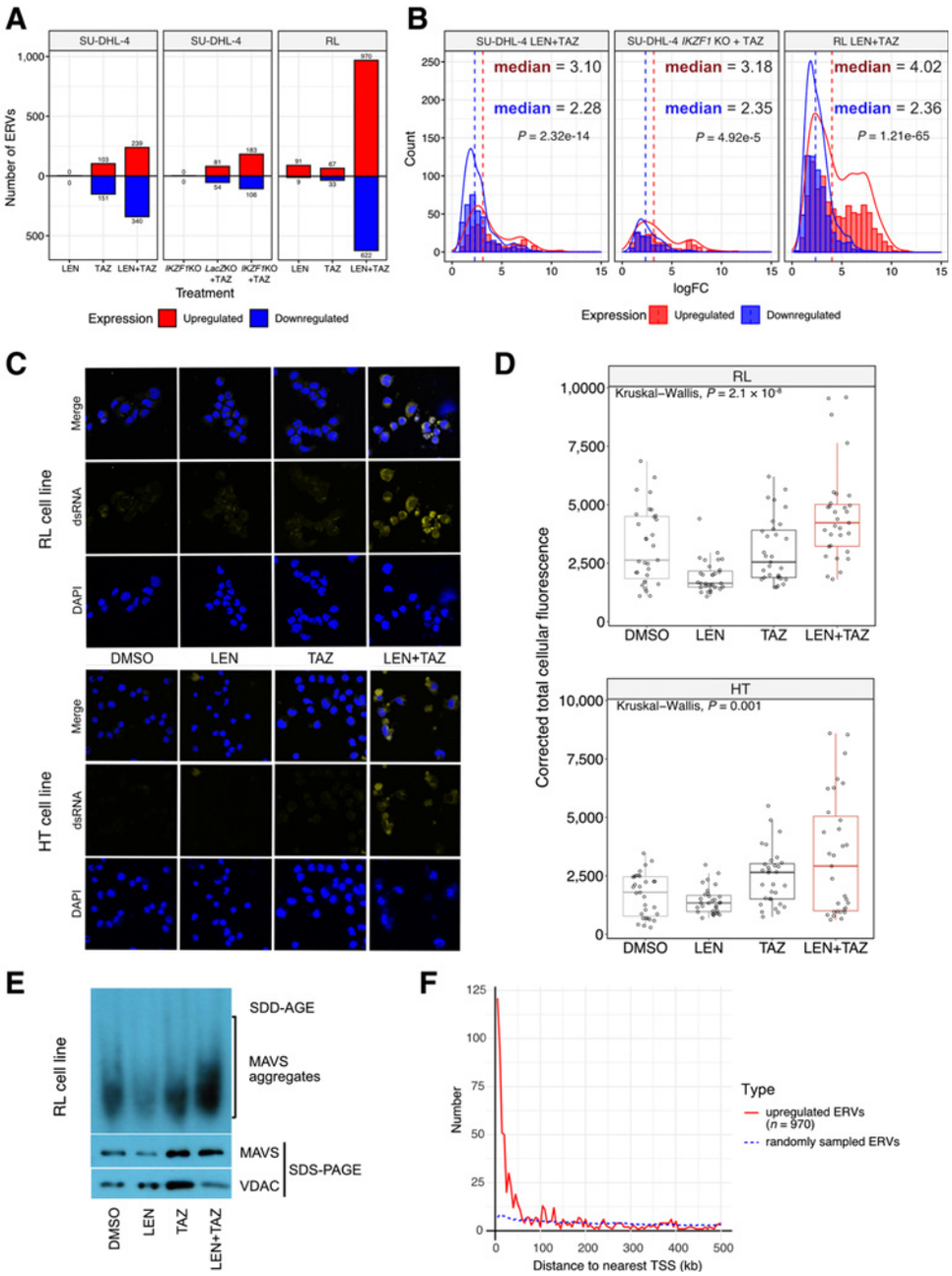

Figure 6.

ERV expression changes correlate with synergy and interferon response. **A,** Summary of significantly differentially expressed ERVs (FDR < 0.05) across the three cell line contexts and three treatments. **B,** Summary of log FCs of significantly differentially expressed ERVs associated with combination treatment across the three cell lines. Median FC is shown for upregulated and downregulated ERVs. **C,** RL or HT cells were treated with either vehicle or drugs for 6 days. Cells were then deposited onto slides and immunostained with dsRNA J2 antibody for detecting global dsRNA (golden yellow). DAPI, nuclear counterstain (blue). **D,** Quantification of immunofluorescence of dsRNA for RL (top) and HT (bottom) cells. Cells ($n = 30$) from two independent experiments of each treatment group were randomly picked and the fluorescent signal was quantified by ImageJ. The corrected total cell fluorescence was calculated as described in the Supplementary Materials and Methods. Data are shown as median with interquartile range of CTCF in the box plots. Comparison between treatment groups were analyzed by Kruskal–Wallis test. DMSO, vehicle control; LEN, 10 μmol/L lenalidomide; TAZ, 5 μmol/L tazemetostat; LEN+TAZ, combination treatment. **E,** Induction of MAVS into functional aggregates on the mitochondrial membrane. Crude mitochondrial extracts prepared from RL cells treated with vehicle or drugs for 4 days were analyzed by SDD-AGE and SDS-PAGE. Data shown are representative of three independent experiments. VDAC (voltage-dependent anion channel), mitochondrial loading control. **F,** Evaluating enrichment of upregulated ERVs near upregulated protein-coding genes in RL combination treatment. The red curve shows the results for ERVs ($n = 970$) while the blue curve shows the average results for the detected ERVs that were not significantly upregulated. The *y*-axis represents the number of ERVs associated with at least one protein-coding gene at a given distance. For example, 121 of 970 ERVs were found to be near at least one upregulated gene (within 5 kb) while for randomly selected ERVs, this number was six.

of ERVs across the three cell-line models and treatments. We focused on ERV families including ERVL, ERV1, ERVK, LTR, and ERVL-MaLR. We observed that the number of differentially expressed ERVs was highest in the comparison between combination treatment and DMSO (**Fig. 6A**), and this effect was most pronounced in the RL cell line. The median FC of upregulated ERVs was higher than the median FC of downregulated genes, and the overall signal was stronger in RL cells treated with lenalidomide and tazemetostat, compared with SU-DHL-4 (**Fig. 6B**). As an orthogonal validation of increased ERV expression with combination treatment, we applied immunofluorescence using an antibody against double-stranded RNA (dsRNA). Using an anti-dsRNA J2 antibody and confocal microscopy, we documented enhanced ERV expression in the HT and RL cell lines, when comparing combination treatment with single-agent treatment or DMSO control (**Fig. 6C** and **D**). Moreover, we isolated the mitochondrial fraction in RL cells and could detect the formation of Mitochondrial Antiviral Signaling Protein (MAVS) aggregates in semi-denaturing conditions (**Fig. 6E**), suggesting activation of cytoplasmic pattern recognition receptors in response to ERV derepression.

Next, we focused on the combination-treated cells and interrogated the distribution of ERVs across the genome in the RL cell line. We found that this distribution was nonrandom and strongly skewed toward upregulated ERVs being located in close vicinity to upregulated protein-coding genes (**Fig. 6F**). On the other hand, for randomly selected ERVs, the enrichment near the transcription start sites of upregulated protein-coding genes was minimal. We could confirm this observation using the GREAT tool (45), with more than 99% of the 970 upregulated ERVs associated with protein-coding genes (Supplementary Fig. S13A, left). There were a total of 1,781 ERV-gene associations spanning 873 unique protein-coding genes and the most common absolute distance to the transcription start site was between 5 and 50 kb (Supplementary Fig. S13A, middle and right). Of these protein-coding genes, 253 (29%) were also significantly upregulated. These genes included *OAS2, DDX58*, and *HLA-B*, and others enriched in pathways such as negative regulation of viral life cycle, IFN signaling, and defense response to virus (Supplementary Fig. S13B; Supplementary Table S5). Annotations of IRF1 were also enriched, which has previously been associated with inducing ERV expression (46). Thus, the observed upregulation of interferon pathways in cells treated with lenalidomide and tazemetostat was associated with increased expression of neighboring ERVs. We explored potential mechanisms leading to markedly increased ERV expression. We observed a significant overlap between upregulated ERVs in combination-treated cells and regions with increased H3K27ac ($P = 0.001$ shown in Supplementary Fig. S14, left). Furthermore, there was also a significant overlap between these ERVs and H3K27me3 regions in untreated lymphoma cell lines ($P = 0.001$ shown in Supplementary Fig. S14, right). These regions reflect baseline H3K27me3 marks and are expected to be demethylated in cells treated with tazemetostat or combination treatment. Thus, our findings showed that combination treatment led to co-expression of ERVs and neighboring genes that have an inflammatory function.

Discussion

Here, we performed an unbiased CRISPR/Cas9 screen to identify genetic determinants of sensitivity to EZH2 inhibition, and uncovered synergy between tazemetostat and lenalidomide that was unexpected in a GCB-DLBCL context. Indeed, lenalidomide has previously been found to be active mostly in ABC-DLBCL (34). Our study supports the use of unbiased screens to identify rational drug combinations, as opposed to clinical development of treatment strategies that is based on inefficient "trial and error" (47). Tazemetostat, in particular, is well suited for combination studies as it is well tolerated and has demonstrated activity in both follicular lymphoma and DLBCL (14, 15). Several preclinical studies have reported promising results combining tazemetostat with glucocorticoid receptor agonists (48), inhibitors of B-cell receptor signaling (19), and HDAC inhibitors (49). Recently, another EZH2 inhibitor (GSK126) was reported to synergize with pomalidomide in *EZH2*-mutant but not wildtype cell lines, an effect that was perceived to be independent of IKAROS transcription factors, in contrast to our findings (50). In our study, we provide insight into the molecular basis underlying synergy between tazemetostat and lenalidomide, showing that combination treatment leads to upregulation of IFN response pathways and ERVs, correlating with concomitant epigenetic changes underlying gene expression. Moreover, our results provide preclinical rationale for a current phase Ib/III trial that randomizes patients into either rituximab and lenalidomide (R2) or R2 combined with tazemetostat (NCT04224493).

IFN responses have previously been linked to immunomodulatory drugs. For example, in ABC-DLBCL, lenalidomide leads to IFNβ production which has an antiproliferative effect (34). Avadomide (CC-122), a more recent cereblon modulator, triggers transcription of IFN-stimulated genes that is independent of cell of origin (51). In parallel, PRC2 has been shown to repress cytokine pathways, including IFN-stimulated genes, in a broad range of solid cancer cell lines (52). Moreover, PRC2 leads to immune evasion through silencing of MHC class I antigen presentation (53), and in DLBCL, EZH2 inhibition allows the restoration of MHC expression (54). Nonetheless, and to the best of our knowledge, our study is the first to describe synergy between tazemetostat and IKAROS inhibition in DLBCL, and to link upregulation of interferon response genes to synergy between these two drugs.

In our study, we report that combination treatment leads to derepression of endogenous retroelements, which has previously been described with demethylating agents in various solid cancers and is often referred to as "viral mimicry" (41–43). Resulting transcripts form dsRNAs that can be detected by RIG-I-like receptors such as *DDX58* or *MDA5*, which in turn can activate the MAVS and subsequently generate an antiviral response (55). The upregulated ERVs induced by combination treatment were not randomly distributed across the genome, but rather enriched in regions marked with H3K27ac and H3K27me3 as well as near genes involved in immune signaling. Of interest, ERVs have previously been described to facilitate expression of neighboring IFN-stimulated genes (56), but, inversely, exogenous IFNγ has also been reported to lead to ERV expression (57). Hence, while ERV derepression is generally considered to secondarily lead to IFN pathway activation, the relationship between these two events may be more nuanced. Our findings support the possibility that the interferon response can be triggered by direct epigenetic mechanisms, resulting from the combined effects of tazemetostat and lenalidomide.

We observed coordinated increases in H3K27ac and differential gene expression that was most significant in combination treatment, followed by single-agent tazemetostat and single-agent lenalidomide. These results suggest that the observed synergy may result from a combined effect on histone acetylation. The increase in H3K27ac with tazemetostat is not unexpected, given that trimethylation and acetylation of H3K27 are inversely correlated at promoters of polycomb group target genes (58). On the other hand, epigenetic effects of lenalidomide are less well described. While the primary mechanism

of action of lenalidomide results from cereblon-dependent degradation of IKAROS proteins (32, 33), both IKAROS and AIOLOS can associate with the NuRD complex (36), and more specifically the histone deacetylases HDAC1 and HDAC2 that are NuRD components (35, 59). Our own ChIP-seq data are consistent with an indirect epigenetic effect of lenalidomide, through degradation of IKAROS proteins and decreased histone deacetylase activity. As our study primarily describes gene expression and epigenetic changes underlying the synergy between EZH2 inhibition and IKAROS degradation, additional studies are warranted to decipher the precise molecular and cellular mechanisms associated with synergy.

In summary, we found unexpected synergy between lenalidomide and tazemetostat in a range of GCB-DLBCL cell lines and *in vivo*, which appeared to be independent of *EZH2* mutation status. Efficacy in immunocompetent hosts can potentially be further enhanced through immune modulation, which could be mediated both by lenalidomide and EZH2 inhibition (54, 60). While an ongoing clinical trial is testing whether the combination therapy is effective in patients with follicular lymphoma, when given with rituximab, our data support clinical studies also in patients with DLBCL.

Authors' Disclosures

K.I. Tong reports grants from Gilead Sciences, Canadian Hematology Society, and Leukemia & Lymphoma Society of Canada, as well as non-financial support from Epizyme during the conduct of the study. S. Yoon reports other support from Canada Graduate Scholarships - Master's (CGS M) during the conduct of the study. K. Isaev reports grants from Gilead Sciences, Canadian Hematology Society, and Leukemia & Lymphoma Society of Canada, as well as non-financial support from Epizyme during the conduct of the study. T. Lackraj reports grants from Gilead Sciences, Canadian Hematology Society, and Leukemia & Lymphoma Society of Canada, as well as non-financial support from Epizyme during the conduct of the study. M.Y. He reports grants from Gilead Sciences, Canadian Hematology Society, and Leukemia & Lymphoma Society of Canada, as well as non-financial support from Epizyme during the conduct of the study. J. Joynt reports grants from Gilead Sciences, Canadian Hematology Society, and Leukemia & Lymphoma Society of Canada, as well as non-financial support from Epizyme during the conduct of the study. A. Silva reports other support from Canadian Institutes of Health Research during the conduct of the study. G.G. Privé reports grants from SWCRF during the conduct of the study. R.E. Tiedemann reports grants from Terry Fox Research Institute and the Canadian Institutes of Health Research outside the submitted work. D.W. Scott reports personal fees from AbbVie, AstraZeneca, Celgene, and Incyte; grants and personal fees from Janssen; and grants from NanoString outside the submitted work. In addition, D.W. Scott has a patent for subtyping lymphoma types by means of expression profiling, pending and licensed to NanoString. C. Steidl reports grants from Terry Fox Research Institute and BC Cancer Foundation during the conduct of the study; C. Steidl also reports personal fees from Seattle Genetics, Curis Inc, Roche, Bayer, and AbbVie, as well as other support from Trillium Therapeutics Inc., Epizyme, and Bristol Myers Squibb outside the submitted work. R. Kridel reports grants from Gilead Sciences, Canadian Hematology Society, and Leukemia & Lymphoma Society of Canada, as well as non-financial support from Epizyme during the conduct of the study and grants from Roche outside the submitted work. No disclosures were reported by the other authors.

Authors' Contributions

K.I. Tong: Conceptualization, formal analysis, validation, investigation, visualization, methodology, writing–original draft, writing–review and editing. **S. Yoon:** Formal analysis, validation, investigation, visualization, writing–original draft. **K. Isaev:** Software, formal analysis, investigation, visualization, writing–original draft, writing–review and editing. **M. Bakhtiari:** Investigation, writing–review and editing. **T. Lackraj:** Validation, investigation, visualization. **M.Y. He:** Writing–review and editing. **J. Joynt:** Investigation. **A. Silva:** Writing–review and editing. **M.C. Xu:** Formal analysis, investigation, writing–review and editing. **G.G. Privé:** Formal analysis, investigation, writing–review and editing. **H.H. He:** Formal analysis, supervision, investigation, writing–review and editing. **R.E. Tiedemann:** Formal analysis, supervision, investigation, writing–review and editing. **E.A. Chavez:** Data curation, formal analysis, investigation. **L.C. Chong:** Data curation, formal analysis, investigation. **M. Boyle:** Resources, formal analysis, supervision, investigation. **D.W. Scott:** Resources, formal analysis, supervision, investigation, writing–review and editing. **C. Steidl:** Resources, formal analysis, supervision, investigation, writing–review and editing. **R. Kridel:** Conceptualization, resources, data curation, formal analysis, supervision, funding acquisition, validation, investigation, visualization, methodology, writing–original draft, project administration, writing–review and editing.

Acknowledgments

We thank Troy Ketela and Princess Margaret Genomics Centre for their assistance with regards to the CRISPR/Cas9 screen and ChIP-seq. We thank Dr. Elisa Oricchio for her valuable insight on ChIP experiments and Natalie Erdmann for her expert advice on immunofluorescence. We would like to thank Dr. Shane Harding and Dr. Sarika Khasnis for their guidance and the use of the ME220 Focused-ultrasonicator. We also acknowledge services from Princess Margaret Bioinformatics and High-Performance Computing Core. Tazemetostat for the *in vivo* studies was generously provided by Epizyme, Inc. This study was supported by funding awarded to R. Kridel including: RK Smiley Research Grant from the Canadian Hematology Society, Operating Grant (grant no. 621322) from the Leukemia and Lymphoma Society of Canada, and support from the Princess Margaret Cancer Foundation. This independent research was also supported by the Gilead Sciences Research Scholars Program in HEM/ONC (to R. Kridel), the Program Project Grant funding from the Terry Fox Research Institute (grant no. 1061, to C. Steidl), and the BC Cancer Foundation (to C. Steidl). S. Yoon holds a NSERC Graduate Scholarship awarded from The Natural Sciences and Engineering Research Council of Canada. A. Silva is a recipient of a Postdoctoral Fellowship awarded from the Canadian Institutes of Health Research.

The costs of publication of this article were defrayed in part by the payment of page charges. This article must therefore be hereby marked *advertisement* in accordance with 18 U.S.C. Section 1734 solely to indicate this fact.

Received October 26, 2020; revised March 24, 2021; accepted June 18, 2021; published first June 24, 2021.

References

1. NIH. SEER. Diffuse large B-cell lymphoma - cancer stat facts. Available from: https://seer.cancer.gov/statfacts/html/dlbcl.html.
2. Crump M, Neelapu SS, Farooq U, Van Den Neste E, Kuruvilla J, Westin J, et al. Outcomes in refractory diffuse large B-cell lymphoma: results from the international SCHOLAR-1 study. Blood 2017;130:1800–8.
3. Neelapu SS, Locke FL, Bartlett NL, Lekakis LJ, Miklos DB, Jacobson CA, et al. Axicabtagene ciloleucel CAR T-cell therapy in refractory large B-cell lymphoma. N Engl J Med 2017;377:2531–44.
4. Morin RD, Johnson NA, Severson TM, Mungall AJ, An J, Goya R, et al. Somatic mutations altering EZH2 (Tyr641) in follicular and diffuse large B-cell lymphomas of germinal-center origin. Nat Genet 2010;42:181–5.
5. Cao R, Wang L, Wang H, Xia L, Erdjument-Bromage H, Tempst P, et al. Role of histone H3 lysine 27 methylation in Polycomb-group silencing. Science 2002; 298:1039–43.
6. Müller J, Hart CM, Francis NJ, Vargas ML, Sengupta A, Wild B, et al. Histone methyltransferase activity of a Drosophila Polycomb group repressor complex. Cell 2002;111:197–208.
7. Czermin B, Melfi R, McCabe D, Seitz V, Imhof A, Pirrotta V. Drosophila enhancer of Zeste/ESC complexes have a histone H3 methyltransferase activity that marks chromosomal Polycomb sites. Cell 2002;111: 185–96.
8. Yap DB, Chu J, Berg T, Schapira M, Cheng S-WG, Moradian A, et al. Somatic mutations at EZH2 Y641 act dominantly through a mechanism of selectively altered PRC2 catalytic activity, to increase H3K27 trimethylation. Blood 2011; 117:2451–9.
9. Béguelin W, Popovic R, Teater M, Jiang Y, Bunting KL, Rosen M, et al. EZH2 is required for germinal center formation and somatic EZH2 mutations promote lymphoid transformation. Cancer Cell 2013;23:677–92.

10. Knutson SK, Wigle TJ, Warholic NM, Sneeringer CJ, Allain CJ, Klaus CR, et al. A selective inhibitor of EZH2 blocks H3K27 methylation and kills mutant lymphoma cells. Nat Chem Biol 2012;8:890–6.
11. McCabe MT, Ott HM, Ganji G, Korenchuk S, Thompson C, Van Aller GS, et al. EZH2 inhibition as a therapeutic strategy for lymphoma with EZH2-activating mutations. Nature 2012;492:108–12.
12. Garapaty-Rao S, Nasveschuk C, Gagnon A, Chan EY, Sandy P, Busby J, et al. Identification of EZH2 and EZH1 small molecule inhibitors with selective impact on diffuse large B cell lymphoma cell growth. Chem Biol 2013;20: 1329–39.
13. Qi W, Chan H, Teng L, Li L, Chuai S, Zhang R, et al. Selective inhibition of Ezh2 by a small molecule inhibitor blocks tumor cells proliferation. Proc Natl Acad Sci U S A 2012;109:21360–5.
14. Morschhauser F, Salles G, McKay P, Tilly H, Schmitt A, Gerecitano J, et al. Interim update from a phase 2 multicenter study of tazemetostat, an EZH2 inhibitor, in patients with relapsed or refractory B-cell non-Hodgkin lymphomas. Hematol Oncol 2017;35:24–5.
15. Morschhauser F, Tilly H, Chaidos A, McKay P, Phillips T, Assouline S, et al. Tazemetostat for patients with relapsed or refractory follicular lymphoma: an open-label, single-arm, multicentre, phase 2 trial. Lancet Oncol 2020;21: 1433–42.
16. Center for Drug Evaluation, Research. FDA granted accelerated approval to tazemetostat for follicular lymphoma; 2020. Available from: https://www.fda.gov/drugs/fda-granted-accelerated-approval-tazemetostat-follicular-lymphoma.
17. Schmitz R, Wright GW, Huang DW, Johnson CA, Phelan JD, Wang JQ, et al. Genetics and pathogenesis of diffuse large B-cell lymphoma. N Engl J Med 2018; 378:1396–407.
18. Chapuy B, Stewart C, Dunford AJ, Kim J, Kamburov A, Redd RA, et al. Molecular subtypes of diffuse large B cell lymphoma are associated with distinct pathogenic mechanisms and outcomes. Nat Med 2018;24:679–90.
19. Brach D, Johnston-Blackwell D, Drew A, Lingaraj T, Motwani V, Warholic NM, et al. EZH2 inhibition by tazemetostat results in altered dependency on B-cell activation signaling in DLBCL. Mol Cancer Ther 2017;16:2586–97.
20. Hart T, Chandrashekhar M, Aregger M, Steinhart Z, Brown KR, MacLeod G, et al. High-resolution CRISPR screens reveal fitness genes and genotype-specific cancer liabilities. Cell 2015;163:1515–26.
21. Li W, Xu H, Xiao T, Cong L, Love MI, Zhang F, et al. MAGeCK enables robust identification of essential genes from genome-scale CRISPR/Cas9 knockout screens. Genome Biol 2014;15:554.
22. Zagidullin B, Aldahdooh J, Zheng S, Wang W, Wang Y, Saad J, et al. DrugComb: an integrative cancer drug combination data portal. Nucleic Acids Res 2019;47: W43–51.
23. Robinson MD, McCarthy DJ, Smyth GK. edgeR: a Bioconductor package for differential expression analysis of digital gene expression data. Bioinformatics 2010;26:139–40.
24. McCarthy DJ, Chen Y, Smyth GK. Differential expression analysis of multifactor RNA-seq experiments with respect to biological variation. Nucleic Acids Res 2012;40:4288–97.
25. Raudvere U, Kolberg L, Kuzmin I, Arak T, Adler P, Peterson H, et al. g:Profiler: a web server for functional enrichment analysis and conversions of gene lists (2019 update). Nucleic Acids Res 2019;47:W191–8.
26. Reimand J, Isserlin R, Voisin V, Kucera M, Tannus-Lopes C, Rostamianfar A, et al. Pathway enrichment analysis and visualization of omics data using g:Profiler, GSEA, Cytoscape and EnrichmentMap. Nat Protoc 2019;14:482–517.
27. Li H, Durbin R. Fast and accurate short read alignment with Burrows-Wheeler transform. Bioinformatics 2009;25:1754–60.
28. Zhang Y, Liu T, Meyer CA, Eeckhoute J, Johnson DS, Bernstein BE, et al. Model-based analysis of ChIP-Seq (MACS). Genome Biol 2008;9:R137.
29. Ross-Innes CS, Stark R, Teschendorff AE, Holmes KA, Ali HR, Dunning MJ, et al. Differential oestrogen receptor binding is associated with clinical outcome in breast cancer. Nature 2012;481:389–93.
30. Yu G, Wang L-G, He Q-Y. ChIPseeker: an R/Bioconductor package for ChIP peak annotation, comparison and visualization. Bioinformatics 2015;31:2382–3.
31. Reddy A, Zhang J, Davis NS, Moffitt AB, Love CL, Waldrop A, et al. Genetic and functional drivers of diffuse large B cell lymphoma. Cell 2017;171:481–94.
32. Krönke J, Udeshi ND, Narla A, Grauman P, Hurst SN, McConkey M, et al. Lenalidomide causes selective degradation of IKZF1 and IKZF3 in multiple myeloma cells. Science 2014;343:301–5.
33. Lu G, Middleton RE, Sun H, Naniong M, Ott CJ, Mitsiades CS, et al. The myeloma drug lenalidomide promotes the cereblon-dependent destruction of Ikaros proteins. Science 2014;343:305–9.
34. Yang Y, Shaffer AL, Tolga Emre NC, Ceribelli M, Zhang M, Wright G, et al. Exploiting synthetic lethality for the therapy of ABC diffuse large B cell lymphoma. Cancer Cell 2012;21:723–37.
35. Song C, Pan X, Ge Z, Gowda C, Ding Y, Li H, et al. Epigenetic regulation of gene expression by Ikaros, HDAC1 and Casein Kinase II in leukemia. Leukemia 2016; 30:1436–40.
36. Kim J, Sif S, Jones B, Jackson A, Koipally J, Heller E, et al. Ikaros DNA-binding proteins direct formation of chromatin remodeling complexes in lymphocytes. Immunity 1999;10:345–55.
37. Hagner PR, Chiu H, Chopra VS, Colombo MS, Patel N, Ortiz M, et al. Interactome of Aiolos/Ikaros in diffuse large B-cell lymphoma (DLBCL) reveals novel combination of cereblon modulators (CELMoD) and histone deacetylase (HDAC) inhibitors. Blood 2019;134(Supplement 1):306.
38. Koipally J, Renold A, Kim J, Georgopoulos K. Repression by Ikaros and Aiolos is mediated through histone deacetylase complexes. EMBO J 1999;18: 3090–100.
39. Creyghton MP, Cheng AW, Welstead GG, Kooistra T, Carey BW, Steine EJ, et al. Histone H3K27ac separates active from poised enhancers and predicts developmental state. Proc Natl Acad Sci U S A 2010;107:21931–6.
40. Qiao Y, Giannopoulou EG, Chan CH, Park S-H, Gong S, Chen J, et al. Synergistic activation of inflammatory cytokine genes by interferon-γ-induced chromatin remodeling and toll-like receptor signaling. Immunity 2013;39:454–69.
41. Roulois D, Loo Yau H, Singhania R, Wang Y, Danesh A, Shen SY, et al. DNA-demethylating agents target colorectal cancer cells by inducing viral mimicry by endogenous transcripts. Cell 2015;162:961–73.
42. Chiappinelli KB, Strissel PL, Desrichard A, Li H, Henke C, Akman B, et al. Inhibiting DNA methylation causes an interferon response in cancer via dsRNA including endogenous retroviruses. Cell 2017;169:361.
43. Liu M, Thomas SL, DeWitt AK, Zhou W, Madaj ZB, Ohtani H, et al. Dual inhibition of DNA and histone methyltransferases increases viral mimicry in ovarian cancer cells. Cancer Res 2018;78:5754–66.
44. Bendall ML, de Mulder M, Iñiguez LP, Lecanda-Sánchez A, Pérez-Losada M, Ostrowski MA, et al. Telescope: characterization of the retrotranscriptome by accurate estimation of transposable element expression. PLoS Comput Biol 2019; 15:e1006453.
45. McLean CY, Bristor D, Hiller M, Clarke SL, Schaar BT, Lowe CB, et al. GREAT improves functional interpretation of cis-regulatory regions. Nat Biotechnol 2010;28:495–501.
46. Manghera M, Ferguson-Parry J, Lin R, Douville RN. NF-κB and IRF1 induce endogenous retrovirus K expression via interferon-stimulated response elements in its 5′ long terminal repeat. J Virol 2016;90:9338–49.
47. Day D, Siu LL. Approaches to modernize the combination drug development paradigm. Genome Med 2016;8:115.
48. Knutson SK, Warholic NM, Johnston LD, Klaus CR, Wigle TJ, Iwanowicz D, et al. Synergistic anti-tumor activity of EZH2 inhibitors and glucocorticoid receptor agonists in models of germinal center non-Hodgkin lymphomas. PLoS One 2014;9:e111840.
49. Lue JK, Prabhu SA, Liu Y, Gonzalez Y, Verma A, Mundi PS, et al. Precision targeting with EZH2 and HDAC inhibitors in epigenetically dysregulated lymphomas. Clin Cancer Res 2019;25:5271–83.
50. Park S, Jo S-H, Kim J-H, Kim S-Y, Ha JD, Hwang JY, et al. Combination treatment with GSK126 and pomalidomide induces B-cell differentiation in gain-of-function mutant diffuse large B-cell lymphoma. Cancers 2020; 12:2541.
51. Hagner PR, Man H-W, Fontanillo C, Wang M, Couto S, Breider M, et al. CC-122, a pleiotropic pathway modifier, mimics an interferon response and has antitumor activity in DLBCL. Blood 2015;126:779–89.
52. Abou El Hassan M, Huang K, Eswara MBK, Zhao M, Song L, Yu T, et al. Cancer cells hijack PRC2 to modify multiple cytokine pathways. PLoS One 2015;10: e0126466.
53. Burr ML, Sparbier CE, Chan KL, Chan Y-C, Kersbergen A, Lam EYN, et al. An evolutionarily conserved function of polycomb silences the MHC class I antigen presentation pathway and enables immune evasion in cancer. Cancer Cell 2019; 36:385–401.
54. Ennishi D, Takata K, Béguelin W, Duns G, Mottok A, Farinha P, et al. Molecular and genetic characterization of MHC deficiency identifies EZH2 as therapeutic target for enhancing immune recognition. Cancer Discov 2019;9: 546–63.
55. Ishak CA, De Carvalho DD. Reactivation of endogenous retroelements in cancer development and therapy. Annu Rev Cancer Biol 2020;4:159–76.

56. Chuong EB, Elde NC, Feschotte C. Regulatory evolution of innate immunity through co-option of endogenous retroviruses. Science 2016;351:1083–7.
57. Cañadas I, Thummalapalli R, Kim JW, Kitajima S, Jenkins RW, Christensen CL, et al. Tumor innate immunity primed by specific interferon-stimulated endogenous retroviruses. Nat Med 2018;24:1143–50.
58. Pasini D, Malatesta M, Jung HR, Walfridsson J, Willer A, Olsson L, et al. Characterization of an antagonistic switch between histone H3 lysine 27 methylation and acetylation in the transcriptional regulation of Polycomb group target genes. Nucleic Acids Res 2010;38:4958–69.
59. Joshi P, Greco TM, Guise AJ, Luo Y, Yu F, Nesvizhskii AI, et al. The functional interactome landscape of the human histone deacetylase family. Mol Syst Biol 2013;9:672.
60. Gribben JG, Fowler N, Morschhauser F. Mechanisms of action of lenalidomide in B-cell non-Hodgkin lymphoma. J Clin Oncol 2015;33:2803–11.
61. Donaldson-Collier MC, Sungalee S, Zufferey M, Tavernari D, Katanayeva N, Battistello E, et al. EZH2 oncogenic mutations drive epigenetic, transcriptional, and structural changes within chromatin domains. Nat Genet 2019;51:517–28.